1-1-2014

Response of the al Σ5〈001〉 left {310} symmetric tilt grain boundary to the shear deformation simulated by molecular dynamics

Kuiyu Cheng
University of Wollongong, kc938@uowmail.edu.au

Cheng Lu
University of Wollongong, chenglu@uow.edu.au

A Kiet Tieu
University of Wollongong, ktieu@uow.edu.au

Response of the al Σ5〈001〉left {310} symmetric tilt grain boundary to the shear deformation simulated by molecular dynamics

Abstract

In the present study, shear response of the Al [001] symmetrical tilting Σ5 (310) grain boundary (GB) was investigated by a three dimensional bicrystal at 500~750 K. It was found that the GB gradually rotated around the [001] tilt axis during the shear deformation due to the combination of surface strain, GB sliding and GB coupled motion. These rotated grain boundaries were Σ5 asymmetrical or symmetrical tilt grain boundaries and led to the normal stress σxx in the bicrystal system. It was also found that the response of the grain boundary to the shear deformation was closely related to the temperatures. At lower temperature (500~650 K), further shear deformation was mediated by crack initiation or dislocation release which is closely related to the local stress condition and temperature etc. The lattice dislocations emitted from GB were identified as pure edge dislocations with Burgers vectors of 〈110〉/2. Interestingly, they have the [001] line direction and glide on the left curly bracket110right curly bracket planes. The reaction between grain boundary and lattice dislocations has been carefully discussed with its role in the shear deformation. At higher temperatures (above 700 K), after a short while of perfect coupling at the early stage the grain boundary quickly rotated and the two grains smoothly slid away from each other in the way of viscous grain boundary sliding under the shear deformation. 2014 by American Scientific Publishers.

Keywords

molecular, 001, 5, al, response, simulated, deformation, shear, boundary, grain, tilt, symmetric, 310, dynamics, left

Disciplines

Engineering | Science and Technology Studies

Publication Details

Cheng, K., Lu, C. & Tieu, K. (2014). Response of the al Σ5〈001〉left {310} symmetric tilt grain boundary to the shear deformation simulated by molecular dynamics. Science of Advanced Materials, 6 (7), 1322-1329.

AMERICAN SCIENTIFIC PUBLISHERS

Science of Advanced Materials
Vol. 6, pp. 1–8, 2014
(www.aspbs.com/sam)

ARTICLE

Response of the Al Σ5 ⟨001⟩ {310} Symmetric Tilt Grain Boundary to the Shear Deformation Simulated by Molecular Dynamics

Kuiyu Cheng, Cheng Lu*, and Kiet Tieu

Faculty of Engineering, University of Wollongong, Northfields, Wollongong, NSW 2500, Australia

ABSTRACT

In the present study, shear response of the Al [001] symmetrical tilting Σ5 (310) grain boundary (GB) was investigated by a three dimensional bicrystal at 500∼750 K. It was found that the GB gradually rotated around the [001] tilt axis during the shear deformation due to the combination of surface strain, GB sliding and GB coupled motion. These rotated grain boundaries were Σ5 asymmetrical or symmetrical tilt grain boundaries and led to the normal stress σ_{xx} in the bicrystal system. It was also found that the response of the grain boundary to the shear deformation was closely related to the temperatures. At lower temperature (500∼650 K), further shear deformation was mediated by crack initiation or dislocation release which is closely related to the local stress condition and temperature etc. The lattice dislocations emitted from GB were identified as pure edge dislocations with Burgers vectors of ⟨110⟩/2. Interestingly, they have the [001] line direction and glide on the {110} planes. The reaction between grain boundary and lattice dislocations has been carefully discussed with its role in the shear deformation. At higher temperatures (above 700 K), after a short while of perfect coupling at the early stage the grain boundary quickly rotated and the two grains smoothly slid away from each other in the way of viscous grain boundary sliding under the shear deformation.

KEYWORDS: Molecular Dynamics, Nanostructured Material, Interface, Grain Boundary Deformation, Coincident Site Lattice.

1. INTRODUCTION

The mechanical response of interfaces plays an ever-more-important role in various properties of both engineering and advanced materials, especially for the nanostructured materials such as bulk nanocrystals,[1] thin films and multilayers,[2–4] nanoporous materials,[5,6] nanowires,[7,8] nanopillars,[9,10] nanopyramids,[11] nanoshperes,[12,13] etc. There into, the interface mediated plastic property and corresponding deformation mechanisms are one of the most fundamental concerns.[14] In recent years, the atomistic simulation method has been found effective at the nano or even smaller scale and has been widely used to investigate the interface mediated plastic deformation which includes grain boundary sliding, coupled motion, emission and annihilation of dislocations at grain boundaries, accommodation of grain boundary atoms, etc.

Chandra and Dang addressed the dependence of grain boundary sliding behaviour on various applied stresses for symmetric tilting grain boundaries and found that the magnitude of the energy barriers is much higher in pure grain boundary sliding than when migration accompanies sliding, and that the grain boundary sliding displacement is proportional to applied force, GB energy, and time.[15] Namilae et al.'s simulations of grain boundary sliding also show a clear dependence of magnitude of sliding on grain boundary energy and more sliding was found at boundaries with higher grain boundary energies for a constant external shear field at a series of [110] symmetric tilting grain boundaries at 448 K.[16] However, Sansoz et al. found that the grain boundary energy alone cannot be used as a relevant parameter to predict the sliding of nanoscale high-angle boundaries when no thermally activated mechanisms are involved and the specific grain boundary structure also plays a significant role.[17] It is also found in a series of studies,[18–20] where grain boundary sliding along a high-symmetry Σ11 [110] (113) tilt GB in Al was investigated, that a perfect grain boundary with the ground-state structure exhibited an extremely high sliding resistance and the extrinsic defects, such as small steps and partial dislocations, reduced the critical stress of sliding by orders of magnitude. Very recently, Qi and Du et al. have proposed that a threshold stress for sliding exists,[21] that the addition of vacancies can decrease the threshold stress for

*Author to whom correspondence should be addressed.
Email: chenglu@uow.edu.au
Received: 1 November 2012
Accepted: 20 May 2013

grain boundary sliding of the low energy grain boundaries by increasing the grain boundary diffusivity but has no effect on high energy grain boundaries[22] and that solution atoms can enhance grain boundary sliding (GBS) in high-energy GBs by weakening Al bonds and by increasing atomic mobility or inhibit GBS by forming atomic clusters and decreasing diffusivity.[23] Besides, it is found that, during grain boundary sliding, disconnections such as ledges and dislocation extensions could inject partials into the grains, which could contribute to the accommodation of the stresses at grain boundaries.[19] Moreover, the dislocation nucleation at twin boundaries can govern the softening and maximum strength in nano-twinned metals,[24] which are more directly related to mechanical behaviour of materials. The MD studies also show that the crack nucleation is preceded by the emission of several dislocations.[25] However, the grain boundary sliding behaviour is very complicated with concurrent accommodation processes, such as grain boundary migration (GBM), coupled motion, maintenance of the grain compatibility, grain rotation, diffusion and dislocation motion. Any variants, like defects or temperatures, can affect the GBS behaviour. Therefore, more detail in the vicinity of the grain boundary should be unveiled.

In the present study, shear response of the Al [001] symmetrical tilting Σ5 (310) grain boundary was simulated at 500∼750 K by molecular dynamics method with a three dimensional bicrystal. Firstly, the simulation method was presented. In the present study, the applied shear force was always perpendicular to the tilt axis. Secondly, the grain boundary evolution during the shear deformation and the reaction between grain boundary and lattice dislocations has been carefully discussed with temperature dependence. The GB rotation was quantitatively determined during the shear deformation and was found to be consistent with the coincident site lattice (CSL) theoretic predictions. At last, the conclusions were drawn from the present study.

2. SIMULATION METHODS

The three dimensional bicrystal model driven by constant shear rate was constructed with the Al [001] symmetrical tilting Σ5 (310) GB and the geometry is illustrated in Figure 1. The simulation system has a dimension of $102.3382 \times 102.3382 \times 51.1691$ Å^3 in $X \times Y \times Z$ and contains 25690 atoms. Periodic boundary condition was applied in the Z-direction which is parallel to the tilt axis and the GB plane, while in the Y-direction the free boundary condition was applied. In the X-direction, the border atoms composed of three-layer atoms at each side were completely fixed in all directions. During the MD simulation, the shear deformation process was realized by moving the fixed atoms of the left grain with the same constant velocity V_y along the Y axis, while the fixed atoms in the right grain remained fixed. The velocity v was determined by different times of the length in the y direction of the simulation block, which were equivalent to 0.2558455 m/s in the present study.

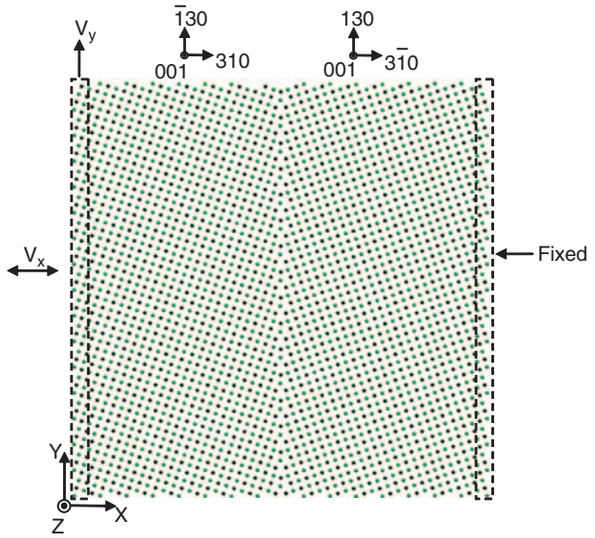

Fig. 1. Geometry of the bicrystal grain boundary sliding model driven by constant shear rate with the Al Σ5 (310) tilting grain boundary. The crystallographic orientations of the bicrystal are also indicated. The green and green with black shadow balls represent rows of atoms with positions in alternating (002) planes.

The MD simulations were carried out using Lammps software[26] with an embedded-atom potential fitted to a large database of experimental and first principles data for Al.[27] This potential has been well tested and shown that it can accurately evaluate a variety of properties of Al, such as the elastic constants, thermal expansion, the intrinsic stacking fault energy, and the coherent twin boundary energy.[27] Simulation temperatures of 500 K, 550 K, 600 K, 650 K, 700 K, and 750 K were selected for the present study to cover the range of interest, and were controlled by the isothermal-isobaric (NPT) ensemble (Nose–Hoover thermostat) with 0 pressures in each direction. The MD integration time step was 1fs. Before the driving force was applied, the bicrystal system was thermally relaxed at the corresponding simulation temperature for 20 ps. The common neighbour analysis (CNA) technique,[28] which classifies all atoms by their local crystallinity, was used to determine and analyse the GB structures in the bi-crystals. The visualisation tools of VMD[29] and AtomEye[30] were used in this work to produce illustrations of the bi-crystal model.

3. RESULTS AND DISCUSSION

3.1. Stress Evolution in the Bicrystal System

Figure 2(a)) shows the evolution of the shear stress σ_{xy} in the bicrystal system during the shear deformation of the Σ5 (310) GB driven by the constant shear rate V_y of 0.2558455 m/s at 500∼750 K. It can be seen that during the shear deformation the shear stress was gradually

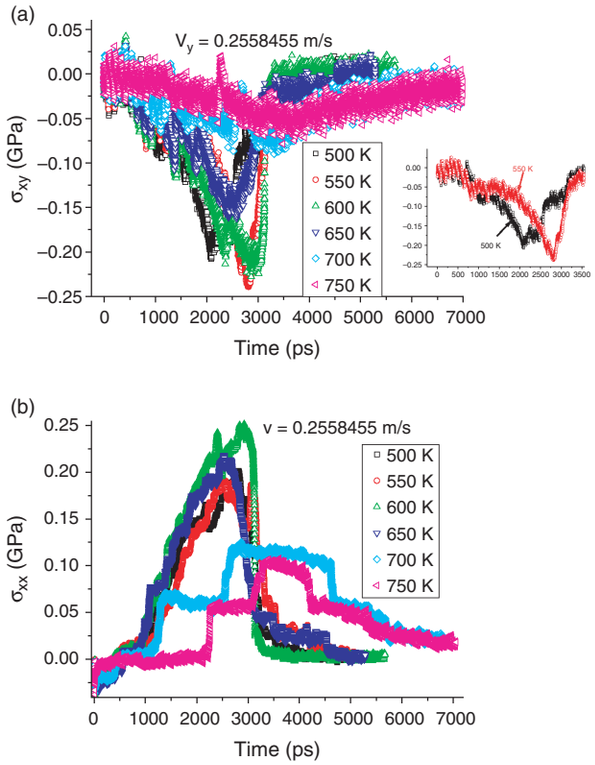

Fig. 2. (a) The shear stress and (b) normal stress caused by the constant shear rate in the whole bicrystal system versus the time of the Σ5 (310) GB at the V_y of 0.2558455 m/s. Insert in (a) shows the curves at 500 K and 550 K separately.

increased up to a peak stress and then decreased gradually at higher temperatures (700∼750 K) or sharply at lower temperatures (500∼650 K) to 0 when the two grains slid away from each other. Moreover, several remarkable features should be noted. Firstly, there is an obvious drop of the peak shear stress between the temperatures of 650 K and 700 K and the peak shear stress is inversely proportional to the temperature. Below 650 K, the peak shear stresses in the bicrystal systems are comparable in the range of 0.18∼0.24 GPa and the largest peak shear stress came up near the temperature of 550∼600 K. However, the peak shear stress reduced to 0.06 GPa when the temperature went up to 700 K. Secondly, the saw-tooth stress characteristic is clearly shown only at the beginning at higher temperatures (700∼750 K), while at lower temperatures (500∼650 K) it is detectable nearly through the whole process of the shear deformation. The normal stress σ_{xx} in the X direction was also monitored during the shear deformation. Interestingly, the shear deformation resulted in a tension of the normal stress σ_{xx} at all temperatures. Below 650 K, the normal stress σ_{xx} increased up with the shear deformation to a peak in tension and then decreased sharply, which is corresponding to the evolution of shear stress in the bicrystal system. Above 700 K, however, there are several nearly flat stages for the normal stress σ_{xx} during the shear deformation and the normal stress σ_{xx} jumps up or drops down very quickly between adjacent stages.

3.2. Evolution of the Atomic Configuration During Shear Deformation

Snapshots of the atomic configuration (projection along the tilt [001] axis) at the concerned stages during shear deformation are shown in Figures 3∼6 to investigate the specific grain boundary deformation behaviour at respective temperatures. At the early stage of 500 K (Figs. 3(a)∼(c)), the inhomogeneous coupled GB motion and migration gradually led to the GB rotation from the initial (310) plane to the (100) plane of left grain and certain pure grain boundary sliding was also accompanied during this process, which can be identified by the discontinuous lattice steps at the top and bottom of the bicrystal. Now, it is readily understood that the normal stress σ_{xx} was caused by the GB rotation. Correspondingly, the shear stress increased to overcome the normal stress on the rotated GB and kept up the same shear rate. The GB rotation angle at early stage of the shear deformation is about 18.435°. It is also worth noting that the saw-tooth characteristic of the shear stress versus time curves (Fig. 2(a)) after the complete GB rotation to the (100) plane of left grain (1350 ps in Fig. 3(c)) is obviously weakened comparing to that before the complete rotation of the GB, which implies that the grain boundary sliding proceeds relatively more smoothly after the GB rotation than before. With further shear deformation, the shear stress was obviously increased and the resolved normal stress formed on the grain boundary due to GB rotation gradually led to an inhomogeneous GB migration. Correspondingly, the GB was further rotated and curved, which also could react the resolved normal stress. Then the

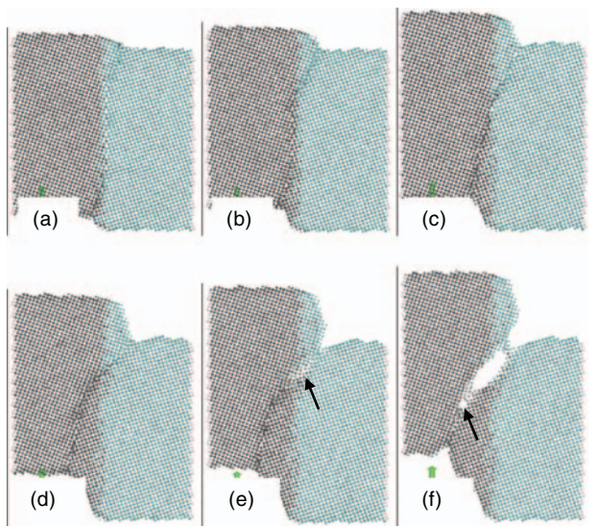

Fig. 3. Snapshots at concerned stages during GBS of the Σ5 (310) at 500 K: (a) 710 ps, (b) 1020 ps, (c) 1350ps, (d) 2020 ps, (e) 2400 ps and (f) 2842 ps. The black arrows indicate the crack initiation.

ARTICLE

proceeding of grain boundary motion or sliding became difficult and the shear stress in the bicrystal reached the peak as expected (2020 ps in Fig. 3(d)). Consequently, in the present case, the crack was initiated from the GB with further shear deformation (2400 ps in Fig. 3(e)) rather than mediating the high shear stress by releasing dislocations, further GB rotation or lattice rotation, and a sharp drop of the shear stress followed. The occurrence of dislocation release or crack initiation at the grain boundary is dependent on the specific orientation relationship (Schmid factor), local stress condition and temperature etc. and it can be very complicated to tell which one would occur first. Therefore, it is most likely in the present case that the critical stress for crack initiation is relatively lower than the critical stresses for other shear deformation mediation manners with respect to the Σ5 (310) GB at 500 K. Moreover, it can be seen in the Figure 3(f) that with further shear deformation instead of only one crack propagation along the grain boundary, another crack initiated from the grain boundary while the first one was propagating in such a small bicrystal system.

At 550 K (Fig. 4), the response of grain boundary to external shear deformation was the most complicated case. First, the GB rotation to the (100) plane of left grain completed very soon under the shear deformation (450 ps in Fig. 4(a)). In this stage, the top surface of the bicrystal shows no obvious lattice steps, which indicates that the upper part experienced nearly pure couple/shear GB motion, while the bottom surface certain lattice steps indicating that a small fraction of GBS occurred in the lower part. Then the GB moved to and fro in a small range with the shear deformation proceeding, which resulted from the dual behaviour of the coupled motion.[31] As shown in Figure 4(b), a large part of the GB from the bottom to the upside nearly rotated back to vertical. In this stage, the shear deformation led to relatively stable GB coupled motion with a little GB sliding. It can also be confirmed by the corresponding shear stress versus time curve between 700∼1500 ps in Figure 2(a), which part is relatively smooth saw-tooth like and nearly horizontal. With further shear deformation (1850 ps in Fig. 4(c)), the GB was further rotated locally and gradually curved as what occurred at 500 K and the shear stress in the system was also increased. Moreover, considerable GB sliding had taken place in this stage. As the shear stress increased with the shear deformation, the uneven GB motion became more obvious due to the more inhomogeneous stress distribution and led to a cusp on the GB (1970 ps in Fig. 4(d)). Interestingly, instead of the crack initiation, a dislocation was nucleated at the cusp to mediate the stress concentration and the cusp area of GB became relative smoother after the dislocation being released from the cusp than before (1983 ps in Fig. 4(e)). After another this process of dislocation nucleation and release (Figs. 4(f) and (g)), a crack finally initiated at the severely rotated GB with a sudden drop of the shear stress (Fig. 4(h)). As mentioned previously, the occurrence of dislocation release or crack initiation at the grain boundary under shear deformation can be very complicated and is dependent on many factors such as the specific orientation relationship, local stress condition and temperature etc. In the present case, it is believed that the dislocation release at the GB rather than crack initiation was mainly due to the 50 K higher temperature than 500 K. Although this difference is not

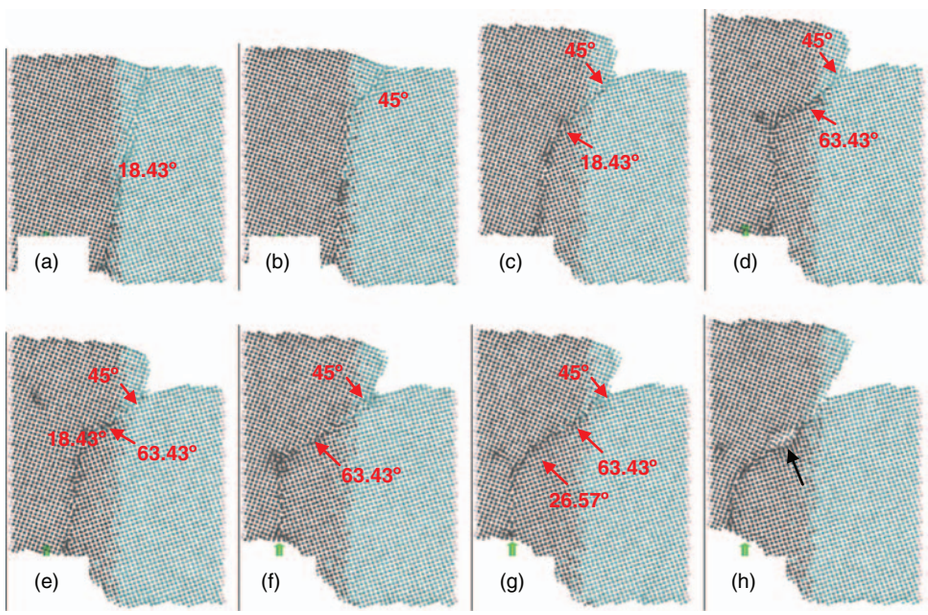

Fig. 4. Snapshots at concerned stages during GBS of the Σ5 (310) at 550 K: (a) 450 ps, (b) 850 ps, (c) 1850 ps, (d) 1970 ps, (e) 1983 ps, (f) 2410 ps, (g) 2421 ps and (h) 2850 ps.

very large, it may increase the atomic activity and help the local atomic accommodation and GB motion or sliding, which might meet the requirements (dislocation nucleation and Schmid factor) for dislocation release. Consequently, as the Schmid factor permitted during GB mediation for the shear deformation, the dislocation may release at the GB and the required shear stress for dislocation release was much low than that for crack initiation (insert in Fig. 2(a)). With further shear deformation, a large part of the GB rotated nearly perpendicular to the external shear stress after two dislocations release, which resulted in large resolved normal stress on this part of GB. Besides, the second dislocation was blocked by the fixed boundary in the vicinity of GB, which would lead to a counterforce on the GB. Therefore, the shear stress kept increasing as well as the normal stress until the crack initiated at the mostly rotated GB. It should be noted that in the practical materials any hard impurities or particular grain boundaries may act as the fixed boundaries. The GB rotation and dislocation formation will be discussed in detail in Sections 3.13 and 3.14 respectively.

The response of grain boundary to external shear deformation at 600 K was similar with that of 650 K and the GB evolution during shear deformation at 600 K is shown in Figure 5. The most representative feature at this temperature range is the perfect coupling motion of GB at the early stage during the shear deformation (Figs. 5(a) and (b)). It can be seen that as the GB moved forward, a sheared lattice was left behind and the initial two grains transited very smoothly across the deformed area without any lattice steps at the top or bottom surface. Moreover, most part of the GB had little rotation at the early stage of the shear deformation. With increasing the shear deformation, the GB gradually rotated to the (100) plane of the left grain as expected and a little GB sliding occurred in this stage (Fig. 5(c)). With further shear deformation, the downside GB obviously rotated as the upside GB reached the fix boundary due to the asymmetrical GB motion (Figs. 5(d) and (e)). The shear stress in the bicrystal system kept building up in this process until the downside GB rotated nearly perpendicular to the external shear force (Fig. 5(e)). Finally, as the most of the GB reached the fixed boundary, the simulation ended. It should be note that no dislocation or crack was found through all the process and the deformation mechanisms were only related to the GB coupled motion or sliding.

Above 700 K, the response of grain boundary to external shear deformation was basically in the way of viscous grain boundary sliding. As shown in Figure 6, after a short while of perfect coupling at the early stage at 750 K the GB quickly rotated about 18.43° and the two grains smoothly slid away from each other on the new GB for a while under the shear deformation (Fig. 6(b)). Then the GB further rotated to 26.57° (Fig. 6(c)) and the grain boundary sliding remained nearly on this new GB until the end of simulation. The relatively stable GB sliding on each GB are completely consistent with the flat stages of the normal stress in Figure 2(b), which further confirm that the normal stress σ_{xx} was caused by the GB rotation and increased with the rotation. Since the GB rotation above 750 K is relatively quick and complete at each stage, the normal stress σ_{xx} curves show flat stages. Subsequently, the shear stress and normal stress were further increased to slide the two grains from each other (Fig. 6(d)). At the

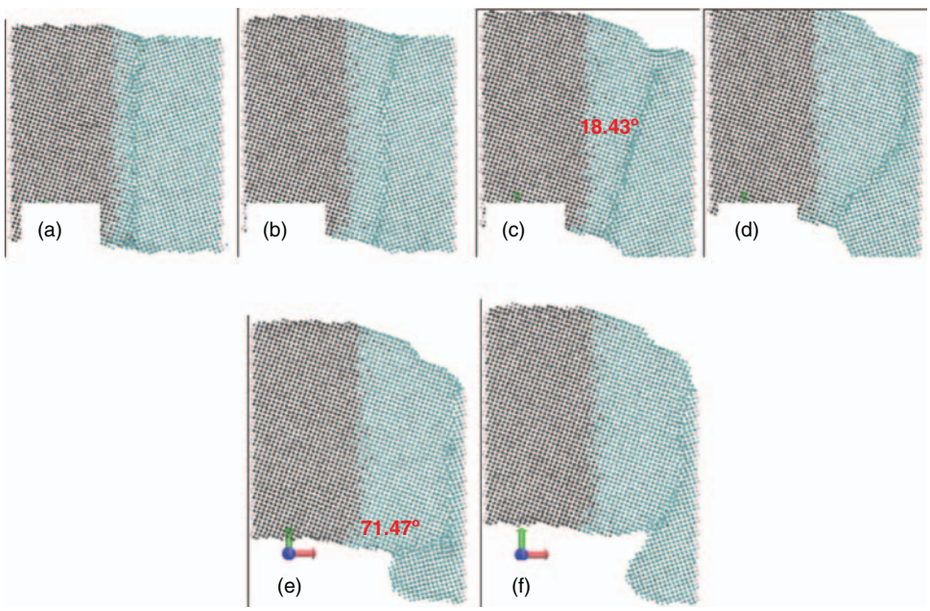

Fig. 5. Snapshots at concerned stages during GBS of the Σ5 (310) at 600 K: (a) 460 ps, (b) 780 ps, (c) 1460 ps, (d) 1950 ps, (e) 2440 ps and (f) 3020 ps.

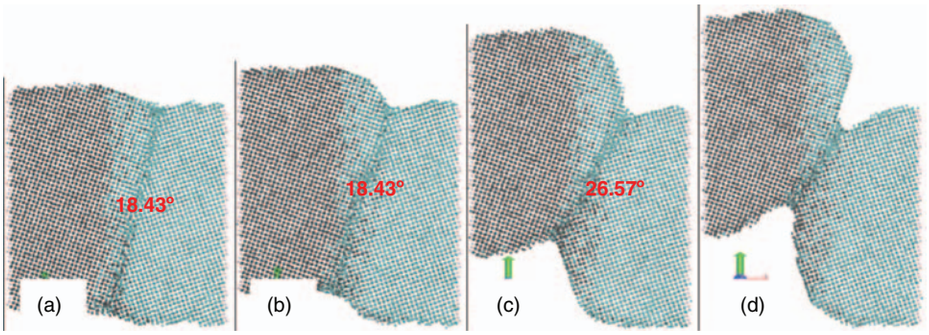

Fig. 6. Snapshots at concerned stages during GBS of the Σ5 (310) at 750 K: (a) 620 ps, (b) 1220 ps, (c) 2700 ps and (d) 3400 ps.

final stage, they were gradually decreased as the grain boundary area shrank.

It can clearly be seen that the response of the GB to the shear deformation is closely related to the temperatures. The temperature directly determines the atom mobility, thereby correspondingly affecting the GB deformation mechanisms including atomic accommodation, shuffling and defects nucleation in the vicinity of the GB. Since the atom colour in the figures represents the atoms belonging to respective grains, the effect of temperature on the atom mobility can be clearly observed by the distance of the atoms diffusing away from the initial GB. In the reference of the left grain, this distance increased obviously with the temperature as shown in the Figures 2∼6. Below 550 K, the black atoms basically stayed at their initial positions except for a few atoms having moved certain distance through the surfaces. However, above 700 K, considerable black atoms had diffused deeply into the right grain after only 620 ps during the shear deformation (Fig. 6(a)). Therefore, at lower temperature the shear deformation is incompletely mediated by local atomic accommodation near the GB and it is readily for lattice defects or cracks to take place to further mediate the shear deformation. However, at higher temperature the shear deformation can be largely mediated by the atomic accommodation or shuffling in several atom layers near the GB and at high enough temperature the GB may even present quasi-liquid (viscous) characteristic, which gives rise to more mobility of the GB and the corresponding macroscopic plasticity of the materials.

3.3. Favourable Grain Boundary Position

If taking a closer look at the curved grain boundaries in Figure 4, it can be seen that the rotated grain boundaries are composed of short flat boundaries rather than being smoothly curved. The angles between these flat boundaries and the original grain boundary are the rotation angles and are indicated on the Figures 4∼6. It is worth noting that all the angles are specific and relevant to the tilt angle θ, which means there are relatively favourable positions for the GB rotation. To explain these favourable GB positions, the coincident site lattice (CSL) of fcc Σ5 grain boundaries is illustrated in Figure 7. The two grains interpenetrate each other and are represented by larger solid cycles for the left grain and smaller outlined cycles for the right grain. The different colours (blue and red) represent rows of atoms with positions in alternating (002) planes. Thus, the larger cycles with smaller rings inside are the coincident sites. For all CSL symmetrical tilt grain boundaries, a rotation of the grain boundary plane about the tilt axis by 45° locates the other CSL symmetrical tilt grain boundary in the ⟨100⟩ system.[32] As shown in Figure 7, an inclination of the boundary plane by 45° from the Σ5 (310) symmetrical tilt grain boundary (vertical or horizontal CSL lines) is the Σ5 (210) symmetrical tilt grain boundary (diagonal lines), while other grain boundaries in between 0° and 45° are Σ5 asymmetric tilt grain boundaries for the ⟨100⟩ system. The black arrows along the CSL indicate some of

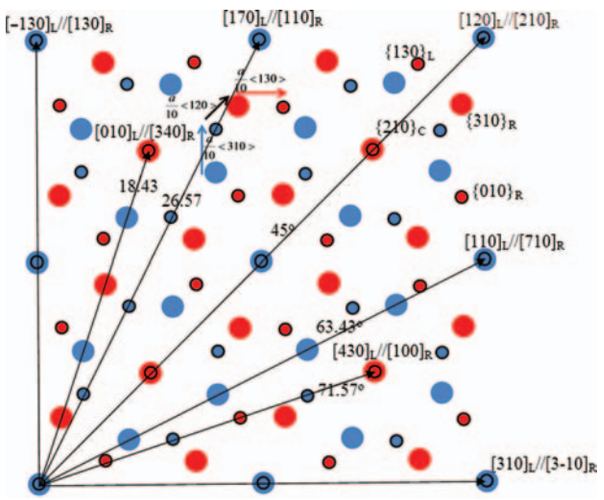

Fig. 7. The dichromatic pattern of the bicrystal for GBs with the misorientation relation given by Σ5 tilt grain boundaries in fcc crystals. The two interpenetrating crystals are represented by larger solid cycles for the left grain and smaller outlined cycles for the right grain. The different colours (blue and red) represent rows of atoms with positions in alternating (002) planes. Larger cycles with smaller rings inside are the coincident sites. The grain boundaries are vertical to the paper and the possible positions are along the black arrows. The indicated angles are referred to the vertical {310} grain boundary.

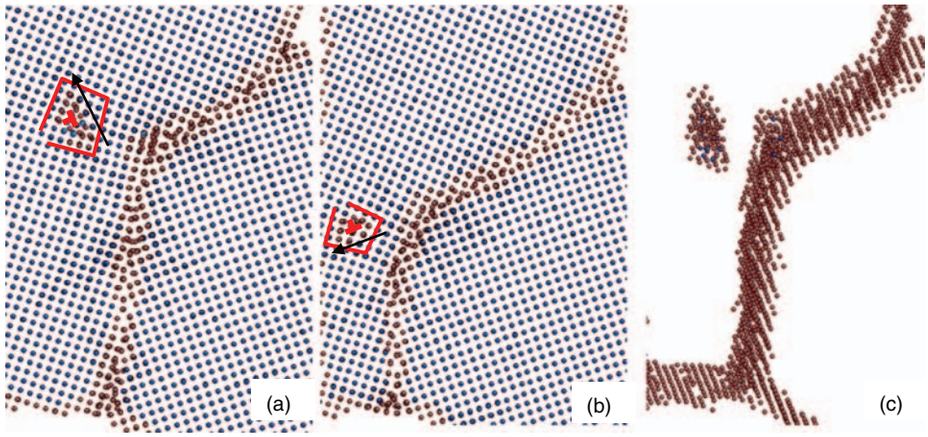

Fig. 8. Lattice dislocations emitted from the grain boundary with Burgers vectors of (a) [−110]/2 at 2014 ps, (b) [−1−10]/2 at 2451 ps and (c) dislocation structure of (a). The red *T* indicates the edge characteristics of the lattice dislocations and the black arrows show the move direction of dislocations.

the Σ5 asymmetrical or symmetrical tilt GB boundaries. It can be seen that the corresponding angles are also consistent with the present simulation. Therefore, the short flat boundaries found in the present study are other Σ5 asymmetrical or symmetrical tilt GB boundaries. As there is litter difference of the grain boundary energies for the Al Σ5 tilt grain boundaries, it is readily for the GB to rotate from one to another one of the Σ5 tilt grain boundaries under external deformation.

3.4. Reaction of the Lattice Dislocation and Grain Boundary Dislocation

To further analyse the dislocation reaction at 550 K, minimization procedure was applied to remove the influence of thermal fluctuation on the atomic positions. Figure 8 shows the detail of dislocation emission from the grain boundary. The atoms are coloured by the common neighbour analysis (CNA) technique:[28] atoms with fcc structural order are blue, atoms with hcp structural order are light blue and atoms with other structural order are red. In the present case, the grain boundary and dislocations are mainly composed of red atoms with very few light blue atoms. Thus, the two examined dislocations are readily identified as pure edge dislocations with Burgers vectors of [−110]/2 (Fig. 8(a)) and [−1−10]/2 (Fig. 8(b)) by Burgers circuit method and the black arrows show the move directions. Combined with the observation in Figure 8(c) where the fcc atoms are removed from the view, it clearly shows that the dislocation line direction is along the [001] tilt axis and the gliding planes are {110} planes. It is known that it is unusual for fcc lattice dislocations to glide on the {110} planes. Therefore their formation must be ascribed to the reaction of grain boundary dislocations. Grain boundary dislocations are very complicated, as they have very specific Burgers vectors that can only occur in grain boundaries. In the present case, the tilt grain boundaries can be simplified as tilt walls of edge dislocations which can be represented with dislocations with alternating perfect lattice Burgers vectors b^A and b^B.[33] Even so, the case is still complicated, as the grain boundary rotated to different Σ5 tilt grain boundaries during shear deformation and then the Burger vectors of the gliding grain boundary dislocations were always changed. However, we may assume all the Burger vectors of the gliding grain boundary dislocations as a common variable [*x y* 0], since all the Burger vectors of the grain boundary dislocations are perpendicular to the tilt axis [001]. Thus, during the shear deformation only the *x* and *y* terms of the Burger vectors are affected by the reaction of grain boundary dislocations. When the grain boundary dislocations are converged by the shear deformation to a point in particular case like at 550 K, it is readily understood that release of the ⟨110⟩/2 lattice dislocations at the grain boundary to mediate the stress concentration is easiest because of their smallest Burgers vectors. For the consistency, the ⟨110⟩/2 lattice dislocations have the [001] line direction and glide on the {110} planes.

4. CONCLUSIONS

Shear response of the Al [001] symmetrical tilting Σ5 (310) grain boundary was simulated by molecular dynamics method with a three dimensional bicrystal at 500∼750 K. Following conclusions can be drawn:

The response of the grain boundary to the shear deformation is closely related to the temperatures. At lower temperature (500∼650 K), the grain boundary responded to the shear deformation by the combination of grain boundary rotation, grain boundary sliding, grain boundary coupled motion, crack initiation or dislocation release. At higher temperatures (above 700 K), after a short while of perfect coupling at the early stage the grain boundary quickly rotated and the two grains smoothly slid away from each other in the way of viscous grain boundary sliding under the shear deformation.

The grain boundary rotated among some of the Σ5 asymmetrical and symmetrical tilt GB boundaries under shear deformation and led to the normal stress σ_{xx} in the bicrystal system.

During shear deformation, reaction of the grain boundary dislocations under particular circumstances could release uncommon edge lattice dislocations from the grain boundary. The uncommon edge lattice dislocations with ⟨110⟩/2 Burgers vectors have the [001] line direction and glide on the {110} planes.

References and Notes

1. Y. Zhang, P. C. Millett, M. Tonks, and B. Biner, *Scripta Mater.* 66, 117 **(2012)**.
2. Y. Zhu, C. F. Tsai, J. Wang, J. H. Kwon, H. Wang, C. V. Varanasi, J. Burke, L. Brunke, and P. N. Barnes, *J. Mater. Res.* 27, 1763 **(2012)**.
3. J. Zheng, R. Yang, Y. Lou, W. Li, and X. Li, *Thin Solid Films* **(2012)**.
4. L. Xue and Y. Han, *Prog. Mater. Sci.* 57, 947 **(2012)**.
5. W. Y. Zhao, Z. Liang, P. Wei, J. Yu, Q. J. Zhang, and G. S. Shao, *Acta Materialia* 60, 1741 **(2012)**.
6. Z. Shao, W. Zhou, and Z. Zhu, *Prog. Mater. Sci.* 57, 804 **(2012)**.
7. C. Xu, J. Wu, U. V. Desai, and D. Gao, *Nano Lett.* 12, 2420 **(2012)**.
8. P. M. Wu, N. Anttu, H. Q. Xu, L. Samuelson, and M. E. Pistol, *Nano Lett.* 12, 1990 **(2012)**.
9. Y. Shibutani, T. Nakano, H. Tanaka, and Y. Kogo, *J. Mater. Res.* 27, 521 **(2012)**.
10. C. S. Roper, A. Gutés, C. Carraro, R. T. Howe, and R. Maboudian, *Nanotechnology* 23 **(2012)**.
11. C. Tournier-Colletta, B. Kierren, Y. Fagot-Revurat, and D. Malterre, *Phys. Rev. Lett.* 104 **(2010)**.
12. X. Zou, J. Liu, Y. Peng, B. Xu, and X. Yu, *J. Nanosci. Nanotechnol.* 12, 2767 **(2012)**.
13. L. Cui, J. Zhu, X. Meng, H. Yin, X. Pan, and S. Ai, *Sens. Actuators, B: Chemical* 161, 641 **(2012)**.
14. Y. Mishin, M. Asta, and J. Li, *Acta Materialia* 58, 1117 **(2010)**.
15. N. Chandra and P. Dang, *J. Mater. Sci.* 34, 655 **(1999)**.
16. S. Namilae, N. Chandra, and T. G. Nieh, *Scripta Materialia* 46, 49 **(2002)**.
17. F. Sansoz and J. F. Molinari, *Acta Materialia* 53, 1931 **(2005)**.
18. R. J. Kurtz, R. G. Hoagland, and J. P. Hirth, *Philosophical Magazine A: Physics of Condensed Matter, Structure, Defects and Mechanical Properties* 79, 683 **(1999)**.
19. R. J. Kurtz, R. G. Hoagland, and J. P. Hirth, *Philosophical Magazine A: Physics of Condensed Matter, Structure, Defects and Mechanical Properties* 79, 665 **(1999)**.
20. R. G. Hoagland and R. J. Kurtz, *Philosophical Magazine A: Physics of Condensed Matter, Structure, Defects and Mechanical Properties* 82, 1073 **(2002)**.
21. Y. Qi and P. E. Krajewski, *Acta Materialia* 55, 1555 **(2007)**.
22. N. Du, Y. Qi, P. E. Krajewski, and A. F. Bower, *Acta Materialia* 58, 4245 **(2010)**.
23. N. Du, Y. Qi, P. E. Krajewski, and A. F. Bower, *Metallurgical and Materials Transactions A: Physical Metallurgy and Materials Science* 42, 651 **(2011)**.
24. X. Li, Y. Wei, L. Lu, K. Lu, and H. Gao, *Nature* 464, 877 **(2010)**.
25. Y. Cheng, M. Mrovec, and P. Gumbsch, *Mater. Sci. Eng., A* 483–484, 329 **(2008)**.
26. S. Plimpton, *Journal of Computational Physics* 117, 1 **(1995)**.
27. Y. Mishin, D. Farkas, M. J. Mehl, and D. A. Papaconstantopoulos, *Physical Review B—Condensed Matter and Materials Physics* 59, 3393 **(1999)**.
28. D. Faken and H. Jónsson, *Computational Materials Science* 2, 279 **(1994)**.
29. W. Humphrey, A. Dalke, and K. Schulten, *Journal of Molecular Graphics* 14, 33 **(1996)**.
30. J. Li, *Modelling and Simulation in Materials Science and Engineering* 11, 173 **(2003)**.
31. J. W. Cahn, Y. Mishin, and A. Suzuki, *Acta Materialia* 54, 4953 **(2006)**.
32. M. A. Tschopp and D. L. McDowell, *Philosophical Magazine* 87, 3871 **(2007)**.
33. J. P. Hirth, R. C. Pond, and J. Lothe, *Acta Materialia* 54, 4237 **(2006)**.